RSC Advances

PAPER

View Article Online
View Journal | View Issue

Published on 23 February 2015. Downloaded by National Sun Yat Sen University on 21/04/2015 09:55:25.

Cite this: *RSC Adv.*, 2015, **5**, 22625

Crystallization ability of poly(lactic acid) block segments in templating poly(ethylene oxide-*b*-lactic acid) diblock copolymers affects the resulting structures of mesoporous silicas

Oleksii Altukhov and Shiao-Wei Kuo*

Received 19th January 2015
Accepted 23rd February 2015

DOI: 10.1039/c5ra01096a

www.rsc.org/advances

In this study we employed poly(ethylene oxide-*b*-lactide) (PEO-*b*-PLA) diblock copolymers as templates to prepare mesoporous silica materials. Small-angle X-ray scattering, transmission electron microscopy, and N_2 adsorption/desorption isotherms revealed that the mesostructures of these mesoporous silicas were influenced by both the tetraethyl orthosilicate content and the volume fraction of the PLA block segment. These effects led to the formation of a variety of composition-dependent mesoporous structures, including hexagonally packed cylinders, face-centered cubic-packed spheres, and disordered spherical micelle structures. When using poly(ethylene oxide-*b*-L-lactide) (PEO-PLLA) diblock copolymers as templates, crystallization of the PLLA block segments was preferred over microphase separation of the block copolymer; accordingly, only lamellar mesoporous structures were formed through crystallization of the PLLA block segment. As a result, eliminating the crystallization ability of PLLA block segments through use of amorphous PLA block segments allowed us to obtain a series of long-range-ordered mesoporous silica materials. As a result, the crystallization ability was the key effect for preparation of highly ordered mesoporous silicas having large pores templated by the PLLA block segment.

Introduction

The self-assembly of block copolymer materials into a number of nanostructures, including lamellae, gyroids, hexagonally packed cylinders, and body-centered cubic spheres, has been studied widely in recent years.[1,2] Likewise, ordered mesoporous materials having high surface areas, large pore volumes, and mechanical stability have also received increasing attention for their potential applications in catalysis, adsorption, photonics, separation, and drug delivery.[3–5] In addition, many studies have been conducted into the formation of mesostructures, using low-molecular-weight poly(ethylene oxide)-*b*-poly(propylene oxide)-*b*-poly(ethylene oxide) (PEO-PPO-PEO) block copolymers as templates, through precipitation-based methods (SBA-*n*).[6–9] The application of this approach has, however, been limited because the low-molecular-weight block copolymers used as templates are soluble only in aqueous systems. Accordingly, an alternative synthetic strategy has been developed involving the templating of mesophase growth during evaporation of volatile solvents; this process, known as evaporation-induced self-assembly (EISA),[10–14] has been used broadly for the preparation of mesoporous materials. EISA facilitates the development of structures through mesophase growth during the process of evaporation of a volatile solvent; subsequent calcination provides the final mesoporous materials.

Many block copolymers have been used as templates for this procedure, usually PEO-based block copolymers; for example, poly(ethylene oxide-*b*-styrene) (PEO-*b*-PS),[15–20] poly(ethylene oxide-*b*-methyl methacrylate) (PEO-*b*-PMMA),[21,22] and poly(ethylene oxide-*b*-isoprene) (PEO-*b*-PI),[23] which can be classified as "crystalline/amorphous" diblock copolymers because PEO forms a crystalline block and PS, PMMA, and PI are all amorphous block segments. In general, when using crystalline/amorphous diblock copolymers as templates to prepare mesoporous materials, the crystalline behavior is relatively unimportant because the PEO block segments usually interact with the mesoporous matrices (*e.g.*, silica, phenolic resin) through hydrogen bonding, thereby decreasing their crystallinity.[24]

In previous studies, we prepared a series of mesoporous silicas, phenolic resins, polybenzoxazine resins, and carbon materials templated by poly(ethylene oxide-*b*-caprolactone) (PEO-*b*-PCL)-based diblock copolymers, which can be classified as crystalline/crystalline diblock copolymer templates.[25–36] Fortunately, we can observe different common mesoporous structures, including lamellae, gyroids, hexagonally packed cylinders, and body-centered cubic spheres, for the mesoporous silicas and phenolic resins templated by such PEO-*b*-PCL

Department of Materials and Optoelectronic Science, Center for Functional Polymers and Supramolecular Materials, National Sun Yat-Sen University, Kaohsiung, Taiwan. E-mail: kuosw@faculty.nsysu.edu.tw

Published on 23 February 2015. Downloaded by National Sun Yat Sen University on 21/04/2015 09:55:25.

diblock copolymers. However, when we change to poly(ethylene oxide-*b*-L-lactide) (PEO-*b*-PLLA) crystalline/crystalline diblock copolymers as templates, we only observe the mesoporous lamellar silicas because the PLLA block segments prefer to crystallize among themselves.[37–39] For crystalline-based diblock copolymers, the formation of well-defined ordered structures is controlled by only three factors: the order-disorder temperature (T_{ODT}), the glass transition temperature (T_g), and the crystallization temperature (T_c).[40] In PEO-*b*-PCL diblock copolymers, the value of T_c of the PCL block (from −50 to +30 °C) is low relative to the value of T_{ODT}; therefore, it does not affect mesostructure formation during the self-assembly process, implying that the free energy of microphase separation is low relative to the crystallization behavior of PCL. The situation changes significantly if the value of T_c of the crystalline block segment is higher; for example, for the PEO-*b*-PLLA crystalline/crystalline diblock copolymer (T_c = 70–130 °C), the free energy of the crystallization process is lower than that for microphase separation and, therefore, we have observed only the lamellar structure arising from PLLA crystallization. To confirm that the crystallization properties do indeed affect the mesoporous structure, we changed the crystalline block to an amorphous block segment. Fortunately, crystalline PLLA can be transformed easily to an amorphous form merely by using a polylactide (PLA) since the equal number of D and L forms; therefore, the polymer overall is not chiral. In addition, the discussion of crystallization effect of PLLA block copolymer as templates to prepare mesoporous silica materials has never reported based on our knowledge. Even some papers already reported PEO-*b*-PLLA block copolymer as templates to prepare mesoporous silica materials, only short-range order of mesoporous structure was observed.[37–39] In addition, PLLA and PLA block copolymers have been studied widely in many fields because of their attractive properties, including biodegradability, biocompatibility, tissue absorbability, microphase separation, and crystallinity.[41,42]

In this present study we focused on the self-assembled structures created during microphase separation within PEO-*b*-PLA diblock copolymers featuring various molecular weights of their PLA block segments. We prepared three PEO-*b*-PLA diblock copolymers of different molecular weights (PEO_{114}-*b*-PLA_{73}, PEO_{114}-*b*-PLA_{130}, PEO_{114}-*b*-PLA_{173}) through simple ring opening polymerization (ROP; Scheme 1); we then prepared mesoporous silicas through EISA, templated by these PEO-*b*-PLA diblock copolymers. We used small-angle X-ray scattering (SAXS), transmission electron microscopy (TEM), and N_2 adsorption/desorption isotherms to investigate the phase behavior of the resulting mesoporous silicas. The merit of this study, we propose another key effect for preparation of highly ordered mesoporous silicas having large pores; such materials might have a range of potential applications in other mesoporous materials.

Experimental

Materials

Monomethoxy-poly(ethylene glycol) having a molecular weight of 5000 (PEO_{114}) and DL-lactide (99%) (Alfa Aesar) were used as received. Xylene was purified through vacuum distillation over CaH_2; the distillation fraction collected at 96–98 °C (5 mm Hg) was used in all polymerization reactions. Stannous(II) octoate [$Sn(Oct)_2$, Sigma] was used as received.

PEO-*b*-PLA copolymers featuring different molecular weights of their PLA block segments

Diblock copolymers were readily prepared through ROP of DL-lactide in the presence of PEO_{114} and $Sn(Oct)_2$ as the catalyst. The reaction mixtures were prepared by introducing a desired volume of DL-lactide monomer into a silanized flask containing a pre-weighed amount of PEO_{114} under a N_2 atmosphere. Several drops of $Sn(Oct)_2$ were added and then the flask was connected to a vacuum line, evacuated, sealed off, and heated at 130 °C. After 24 h, the resulting block copolymers were dissolved in CH_2Cl_2 and precipitated in an excess of cold *n*-hexane with Et_2O. The polymers were dried at 40 °C under vacuum. The characteristics of the diblock copolymers used in this study are summarized in Table 1.

Mesoporous silicas templated by PEO-*b*-PLA copolymers

Mesoporous silicas were prepared through an EISA strategy in THF, using the various PEO-*b*-PLA diblock copolymers (Table 1) as templates and TEOS as the silica precursor (Scheme 2). In a typical synthesis, at a constant concentration of HCl (0.012 g of 0.1 M HCl/PEO-*b*-PLA), a mixture of TEOS and HCl (at a specific

Table 1 Characterization of PEO-*b*-PCL diblock copolymers used in this study

Sample	$M_{n\ (NMR)}$[a]	$M_{n\ (GPC)}$[b]	$M_w/M_{n\ (GPC)}$[b]
PEO_{114}-*b*-PLA_{73}	5256	7200	1.04
PEO_{114}-*b*-PLA_{130}	9432	12 000	1.12
PEO_{114}-*b*-PLA_{173}	12 436	15 000	1.16

[a] Determined using ^1H NMR spectroscopy. [b] Determined using GPC (solvent: DMF; flow rate: 0.6 mL min^{-1}; calibration: PS standards).

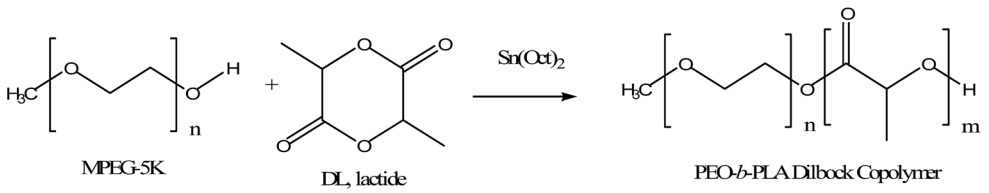

Scheme 1 Synthesis of PEO-*b*-PLA diblock copolymers through ROP.

 This journal is © The Royal Society of Chemistry 2015

Published on 23 February 2015. Downloaded by National Sun Yat Sen University on 21/04/2015 09:55:25.

composition) was added into a stirred solution of PEO-*b*-PLA (2 wt%, containing 0.10 g of copolymer) in THF (5 g); stirring was continued for 30 min to form a homogeneous solution. The sample was poured into a Petri dish and then the THF was evaporated at room temperature for 48 h. The transparent film was collected, ground into a powder, transferred to a PFA bottle containing 1.0 M HCl (30 mL), and treated hydrothermally at 100 °C for 3 days. The product was washed with water and EtOH, dried at room temperature, and calcined in air at 600 °C for 6 h to produce a white mesoporous silica. Calcination processes were conducted in a furnace operated at a heating rate of 1 °C min^{-1}.

Characterization

^{1}H NMR spectra were recorded at room temperature using a Bruker AM 500 (500 MHz) spectrometer, with the residual proton resonance of the deuterated solvent ($CDCl_3$) as the internal standard. Molecular weights and molecular weight distributions were determined through gel permeation chromatography (GPC) using a Waters 510 HPLC equipped with a 410 Differential Refractometer and three Ultrastyragel columns connected in series; DMF was the eluent, at a flow rate of 1.0 mL min^{-1}. SAXS was performed using a NANOSTAR U small-angle X-ray scattering system (Bruker AXS, Karlsruhe, Germany) and Cu-Kα radiation (30 W, 50 kV, 600 mA). The *d*-spacing was calculated using the formula $d = 2\pi/q$, where q is the scattering vector. TEM images were recorded using a JEOL 3010 microscope operated at 200 kV; samples for TEM measurement were suspended in EtOH and supported onto a holey carbon film on a Cu grid. Nitrogen adsorption/desorption isotherms were measured at −196 °C using an ASAP 2020 analyzer; prior to measurement, the samples were degassed under vacuum at 200 °C for at least 6 h. The Brunauer–Emmett–Teller (BET) method was used to calculate specific surface areas and pore volumes; pore size distributions were derived from the adsorption branches of the isotherms through use of the Broekhoff–de Boer (BdB) model.

Results and discussion

Synthesis of PEO-*b*-PLA diblock copolymers

PEO-*b*-PLA diblock copolymers of high molecular weights (Table 1) were readily prepared using a simple one-step ROP

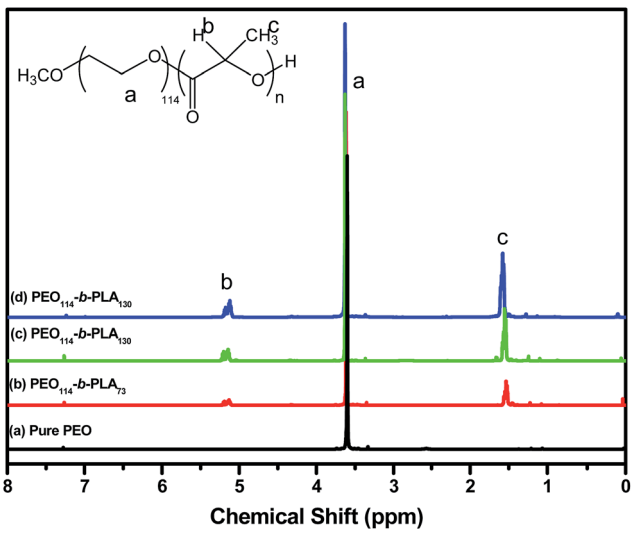

Fig. 1 ^{1}H NMR spectra of PEO-*b*-PLA diblock copolymers (solvent: $CDCl_3$).

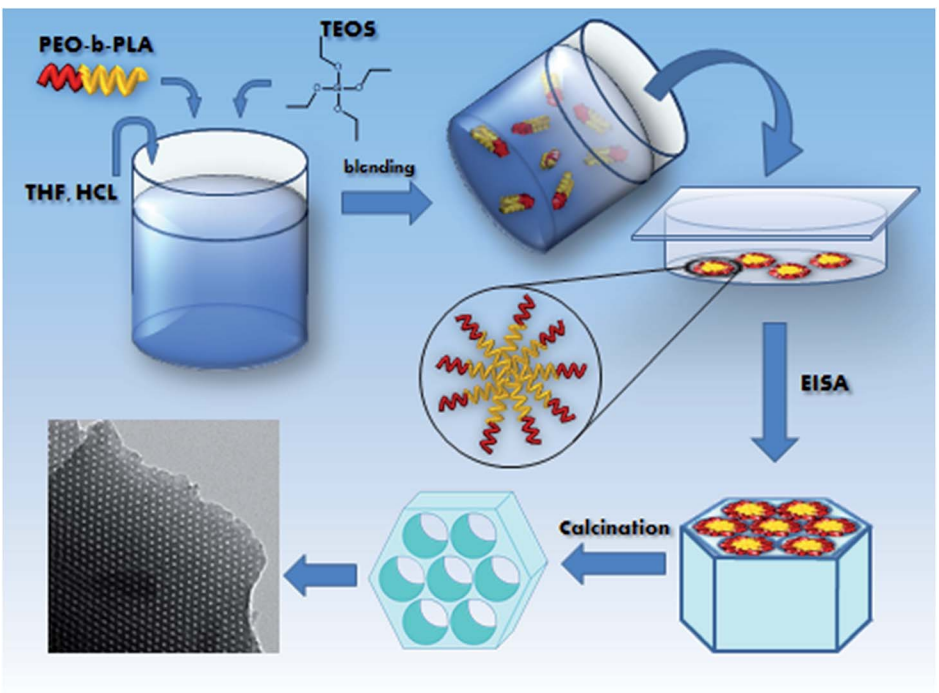

Scheme 2 Preparation of mesoporous silicas, templated by PEO-*b*-PLA diblock copolymers, through the EISA method.

Published on 23 February 2015. Downloaded by National Sun Yat Sen University on 21/04/2015 09:55:25.

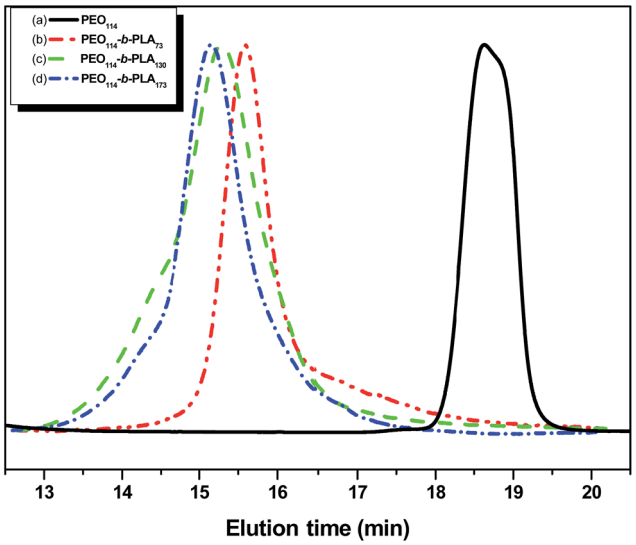

Fig. 2 GPC traces of (a) the homopolymer PEO_{114} and (b–d) the diblock copolymers (b) PEO_{114}-*b*-PLA_{73}, (c) PEO_{114}-*b*-PLA_{130}, and (d) PEO_{114}-*b*-PLA_{173}.

method (Scheme 1). The number-average molecular weights (M_n) of the prepared copolymers were determined from their ^1H NMR spectra by comparing the peak intensity of MPEG-5K ($-CH_2CH_2O-$; δ = 3.65 ppm) to that of PLA ($-C-CH_3-$; δ = 1.60 ppm) and considering the known molecular weight (M_n = 5000) of MPEG-5K (Fig. 1). Block copolymers prepared from the MPEG macroinitiator resulted in products of narrow polydispersity and high symmetry, providing monomodal GPC traces (Fig. 2). The absence of signals for the MPEG-5K macroinitiator supported the formation of the PEO-*b*-PLA diblock copolymers, with the peak maxima of these spectra clearly shifting to higher molecular weight upon increasing the ratio of lactide monomer to MPEG-5K macroinitiator. GPC revealed polydispersity indices (PDIs) of 1.04, 1.12, and 1.16 for PEO_{114}-*b*-PLA_{73}, PEO_{114}-*b*-PLA_{130}, and PEO_{114}-*b*-PLA_{173}, respectively; that is, they each had a narrow molecular weight distribution (Fig. 2).

Mesoporous silicas templated by PEO-*b*-PLA diblock copolymers using the EISA method

We prepared mesoporous silicas through an EISA strategy in THF, using various PEO-*b*-PLA diblock copolymers as templates

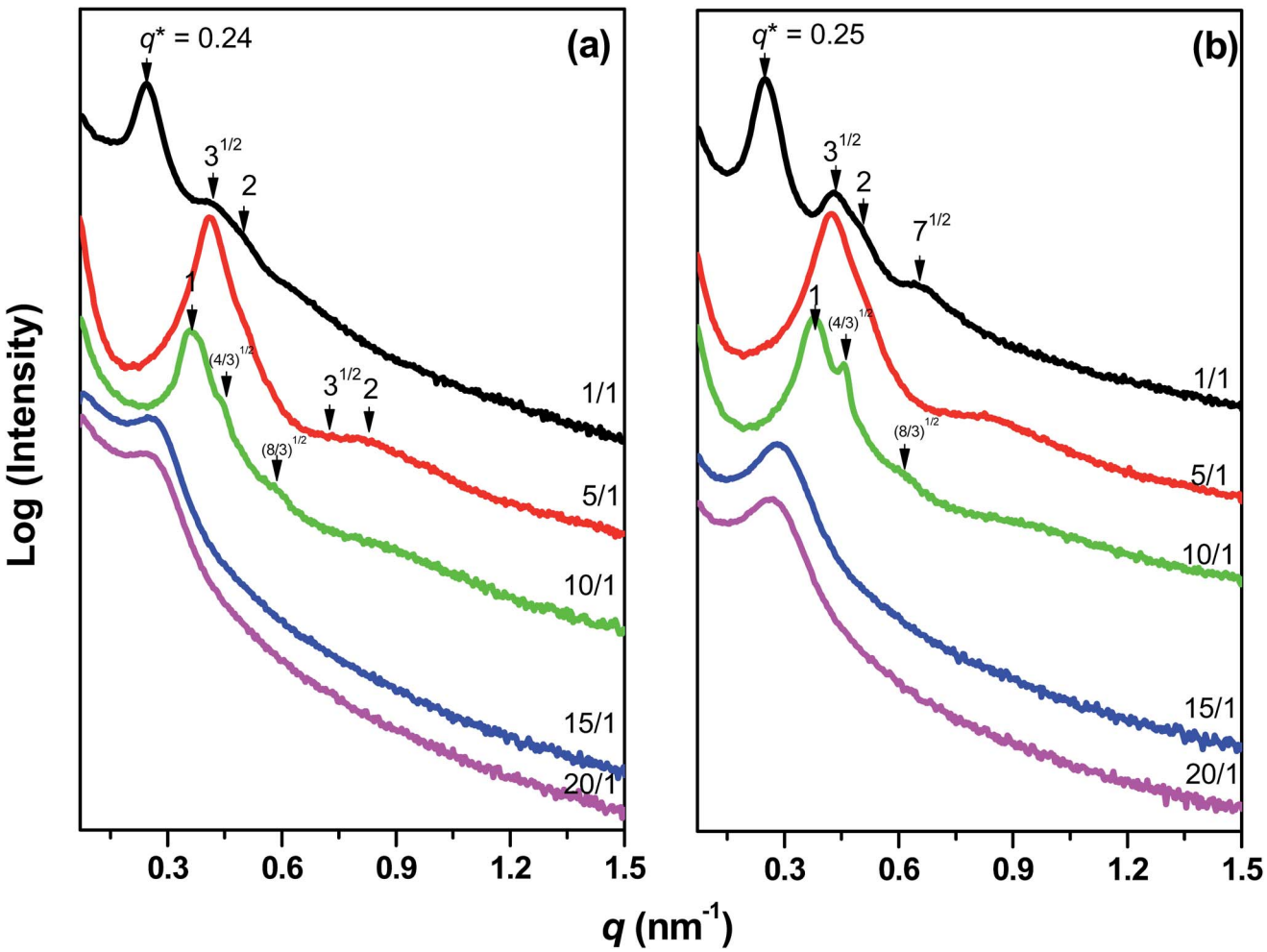

Fig. 3 SAXS patterns of TEOS/PEO_{114}-*b*-PLA_{131} systems prepared at various TEOS-to-PEO-*b*-PLA weight ratios: (a) after hydrothermal treatment; (b) after calcination.

This journal is © The Royal Society of Chemistry 2015

Published on 23 February 2015. Downloaded by National Sun Yat Sen University on 21/04/2015 09:55:25.

and TEOS as the silica precursor (Scheme 2). We recorded SAXS profiles of the TEOS/PEO-*b*-PLA mixtures after their sol–gel reactions to confirm the formation of self-organized morphologies [Fig. 3(a)]. For a ratio of TEOS/PEO_{114}-*b*-PLA_{130} of 1 : 1, we observed q/q_{max} ratios of $1 : \sqrt{3} : \sqrt{4}$ corresponding to the long-range order of a hexagonally packed cylinder structure. Increasing the ratio of TEOS/PEO-*b*-PLA to 5 : 1 resulted in the loss of the long-range-ordered structure, with a weak peak ratio of $1 : \sqrt{3} : \sqrt{4}$, also corresponding to a hexagonally packed cylinder structure. Notably, increasing the TEOS/PEO-*b*-PLA ratio further to 10 : 1 resulted in a face-centered cubic (FCC) lattice, identified by characteristic peak positions in a $1 : \sqrt{4/3} : \sqrt{8/3}$ ratio. When the ratio of TEOS/PEO-*b*-PLA was 15 : 1 or 20 : 1, we observed only single broad peaks through SAXS analyses, indicating the near-disordered and short/long-ordered morphologies of disordered spherical and micelle structures, respectively. In addition, according to the positions of the first-order scattering peaks for the samples containing TEOS/PEO-*b*-PLA at ratios of 1 : 1, 5 : 1, 10 : 1, 15 : 1, and 20 : 1, the average spacing between the neighboring microdomains were 25.3, 15.3, 17.9, 24.7, and 24.7 nm, respectively, indicating that the size of the microphase domains decreased initially but increased thereafter upon increasing the TEOS content. We observed similar trends in the SAXS patterns of our other PEO-*b*-PLA block copolymer templates. After performing the sol–gel processes, we used calcination to remove the PEO-*b*-PLA templates and construct the mesoporous silicas [Fig. 3(b)]. The scattering patterns after hydrothermal treatment and after calcination were identical, except that the higher-order reflection peak became sharper upon removal of the PEO-*b*-PLA diblock copolymer templates, leading to pore formation and greater contrast in electron density. In addition, the first peak shifted to a higher value of q after calcination, due to shrinkage during calcination.

Mesoporous silicas templated by various PEO-*b*-PLA copolymers at different TEOS-to-PEO-*b*-PLA weight ratios

To further understand the phase behavior of the mesoporous silicas templated by the PEO-*b*-PLA copolymers, we used SAXS

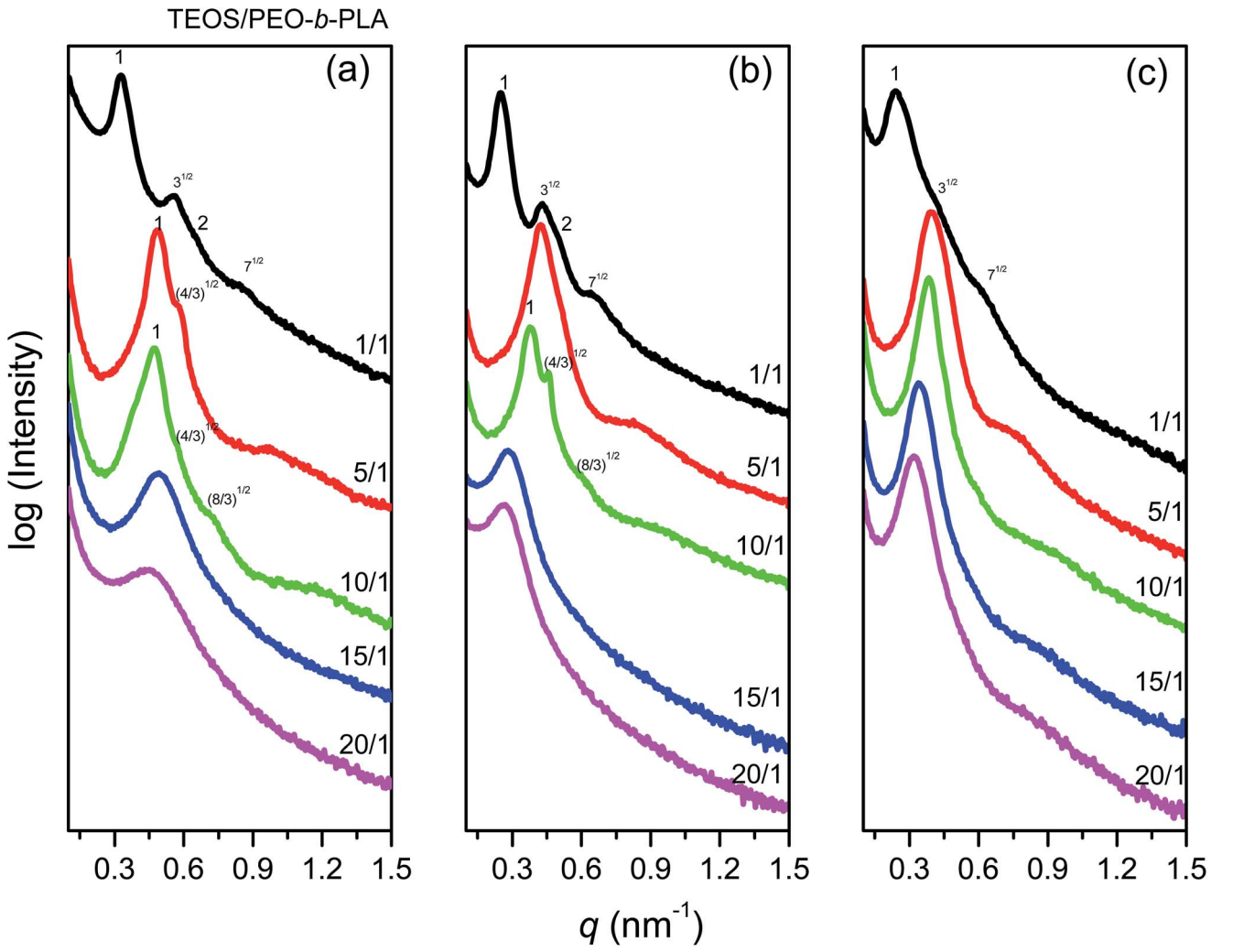

Fig. 4 SAXS patterns of mesoporous silica templated by the diblock copolymers (a) PEO_{114}-*b*-PLA_{73}, (b) PEO_{114}-*b*-PLA_{130}, and (c) PEO_{114}-*b*-PLA_{173}.

Published on 23 February 2015. Downloaded by National Sun Yat Sen University on 21/04/2015 09:55:25.

(Fig. 4) and TEM (Fig. 5) analyses to identify and characterize a series of mesoporous silicas prepared at various TEOS-to-PEO-*b*-PLA weight ratios, with our three PEO-*b*-PLA copolymers (PEO_{114}-*b*-PLA_{73}, PEO_{114}-*b*-PLA_{130}, PEO_{114}-*b*-PLA_{173}) as templates. According to the positions of the first-order scattering peaks in the SAXS patterns (Fig. 4), the average spacing between the neighboring microdomains, corresponding to the average size of the mesoporous silica domains, increased upon increasing the molecular weight of the PLA blocks in the PEO-*b*-PLA copolymers for all individual weight ratios, as revealed in Table 2. For TEOS/PEO_{114}-*b*-PLA_{73} = 1 : 1 [Fig. 4(a)], we observed long-range order at q/q_{max} ratios of 1 : $\sqrt{3}$: $\sqrt{4}$, corresponding to the long-range order of a hexagonally packed cylinder structure, as confirmed in the TEM images in Fig. 5(a). Increasing the TEOS/PEO_{114}-*b*-PLA_{73} ratio to 5 : 1, the scattering peaks shifted toward a specific position at 1 : $\sqrt{4/3}$: $\sqrt{8/3}$, indicating the development of representative FCC packing, as confirmed in the TEM image in Fig. 5(b), suggesting that PEO_{114}-*b*-PLA_{73} was the most suitable template for the structural transition. Increasing the TEOS/PEO_{114}-*b*-PLA_{73} ratio to 10 : 1 led to the scattering peaks also revealing a specific peak ratio of 1 : $\sqrt{4/3}$: $\sqrt{8/3}$, indicating FCC packing, as confirmed in the TEM image in Fig. 5(c). When the TEOS/PEO_{114}-*b*-PLA_{73} ratios were 15 : 1 and 20 : 1, only single broad peaks appeared in the SAXS analyses, suggesting the short/long-ordered morphologies of disordered spherical and micelle structures, respectively [Fig. 5(d)].

In addition, we also investigated the mesostructures that formed when using different weight ratios of TEOS and PEO_{114}-*b*-PLA_{130} (Fig. 3). At a TEOS/PEO-*b*-PLA ratio of 1 : 1, we also observed long-range order at q/q_{max} ratios of 1 : $\sqrt{3}$: $\sqrt{4}$, corresponding to the long-range order of a hexagonally packed cylinder structure, as confirmed in the TEM image in Fig. 5(e). Increasing the TEOS/PEO-*b*-PLA ratio to 5 : 1 led to a weak peak ratio of 1 : $\sqrt{3}$: $\sqrt{4}$, also corresponding to the hexagonally packed cylinder structure revealed through TEM imaging in Fig. 5(f). Notably, increasing the TEOS/PEO-*b*-PLA ratio further to 10 : 1 resulted in an FCC lattice, identified by characteristic peak positions in a 1 : $\sqrt{4/3}$: $\sqrt{8/3}$ ration, as confirmed through TEM imaging [Fig. 5(g)]. The SAXS pattern [Fig. 6(a)] of the FCC-type mesoporous silica formed at a TEOS/PEO_{114}-*b*-PLA_{130} ratio of 10 : 1 exhibited a strong reflection having a *d*-spacing of 16.2 nm, a strong reflection at a value of *q* of 0.44 nm^{-1}, and a weaker reflection at a value of *q* of 0.62 nm^{-1}; this SAXS pattern could be indexed as having (111), (200), and (220) reflections, corresponding to an FCC structure. Fig. 6(b)–(d) display TEM images of the FCC-type mesoporous silica with different orientations ([100], [110], and [211] planes, respectively), consistent with a three-dimensional (3D) cubic cage structure having a large *d*-spacing. We obtained further information

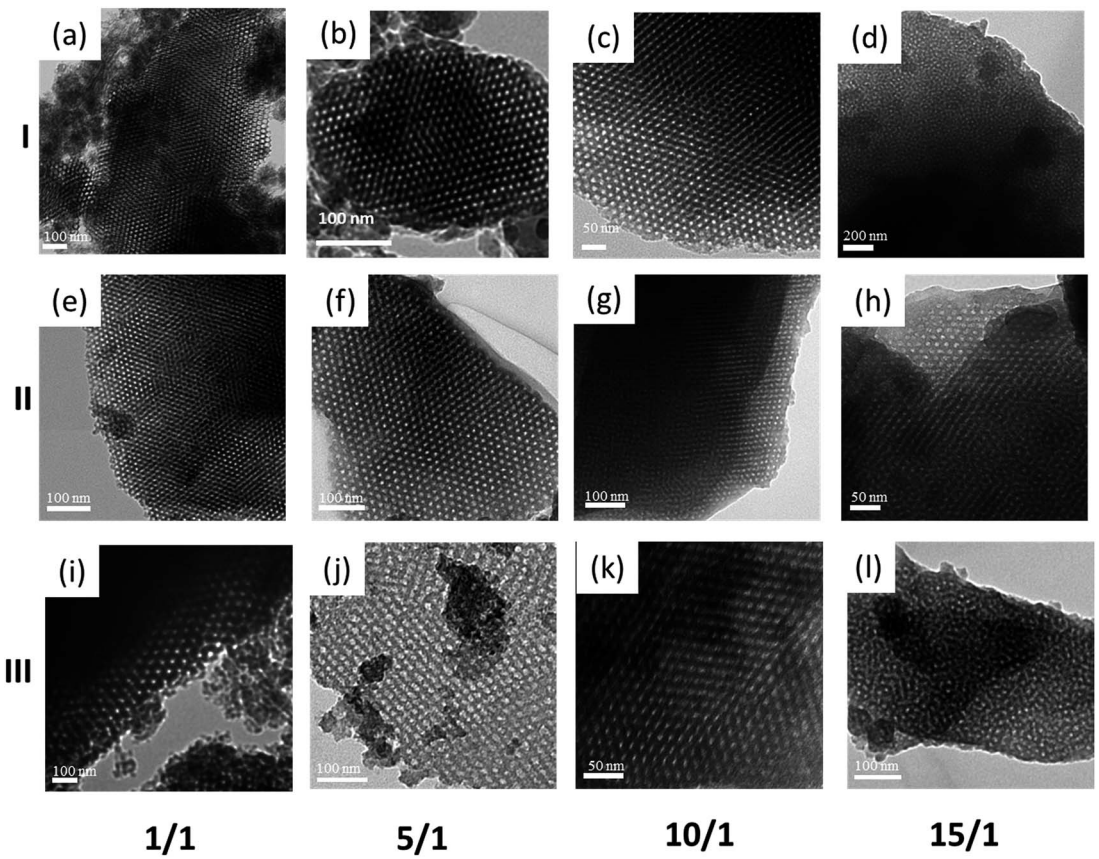

Fig. 5 TEM images of mesoporous silicas templated by the diblock copolymers (I) PEO_{114}-*b*-PLA_{73}, (II) PEO_{114}-*b*-PLA_{130}, and (III) PEO_{114}-*b*-PLA_{173}.

 This journal is © The Royal Society of Chemistry 2015

Published on 23 February 2015. Downloaded by National Sun Yat Sen University on 21/04/2015 09:55:25.

Table 2 Textural properties of mesoporous silicas templated using various block copolymers

Sample	d^a (nm)	Pore size (nm)	$S_{BET}{}^b$ (m^2 g^{-1})	Pore volume (cm^3 g^{-1})	TEOS/template (weight fraction)
1	19.1	16.5	938	2.37	TEOS/PEO_{114}-*b*-PLA_{73} = 1 : 1
2	12.9	5.7	477	0.37	TEOS/PEO_{114}-*b*-PLA_{73} = 5 : 1
3	13.3	5.2	316	0.22	TEOS/PEO_{114}-*b*-PLA_{73} = 10 : 1
4	12.8	4.3	383	0.26	TEOS/PEO_{114}-*b*-PLA_{73} = 15 : 1
5	13.9	4	334	0.23	TEOS/PEO_{114}-*b*-PLA_{73} = 20 : 1
6	25.1	24	547	1.35	TEOS/PEO_{114}-*b*-PLA_{130} = 1 : 1
7	15.0	7.3	473	0.42	TEOS/PEO_{114}-*b*-PLA_{130} = 5 : 1
8	16.6	7.1	423	0.32	TEOS/PEO_{114}-*b*-PLA_{130} = 10 : 1
9	22.3	11.9	328	0.28	TEOS/PEO_{114}-*b*-PLA_{130} = 15 : 1
10	23.7	12.8	279	0.23	TEOS/PEO_{114}-*b*-PLA_{130} = 20 : 1
11	26.2	24.7	639	1.74	TEOS/PEO_{114}-*b*-PLA_{173} = 1 : 1
12	15.9	9.5	467	0.48	TEOS/PEO_{114}-*b*-PLA_{173} = 5 : 1
13	16.5	7.8	348	0.29	TEOS/PEO_{114}-*b*-PLA_{173} = 10 : 1
14	19.6	9	260	0.21	TEOS/PEO_{114}-*b*-PLA_{173} = 20 : 1

^{a} Calculated from the first SAXS peak using the formula $d = 2\pi/q^*$. ^{b} Total BET surface area, calculated from the adsorption branch of the isotherm curve.

regarding the textural properties of the materials from N_2 adsorption/desorption isotherms measured at 77 K. Fig. 6(e) presents the N_2 sorption isotherms of the FCC mesoporous silica sample; the individual type-IV isotherms exhibit an apparent H_2 hysteresis loop, characteristic of a cage-like mesoporous material. A sharp capillary condensation step appeared for this sample, suggesting uniform pore dimensions and high-quality ordering of the material, in agreement with the TEM and SAXS data. Pore size distribution analysis revealed [Fig. 6(f)] a well-ordered cubic structure having pores with an average diameter of approximately 6.7 nm. When the TEOS/PEO-*b*-PLA ratios were 15 : 1 and 20 : 1, SAXS analyses revealed only single broad peaks, indicating the short/long-ordered morphologies of disordered spherical and micelle structures, respectively, as displayed in Fig. 5(h).

Next, we turned our attention to the mesostructures formed from different weight ratios of TEOS and PEO_{114}-*b*-PLA_{173}, which had the highest molecular weight of the PLA block copolymer among our three tested diblock copolymers. We observed relatively less ordered patterns, suggesting that the high molecular weight of PLA in this diblock copolymer was not suitable for the preparation of mesoporous silicas in this study. In Fig. 4(c), for a TEOS/PEO_{114}-*b*-PLA_{173} ratio of 1 : 1, we observed q/q_{max} ratios of 1 : $\sqrt{3}$: $\sqrt{7}$ corresponding to the short-range order of a hexagonally packed cylinder structure, as confirmed by the TEM images in Fig. 5(i). Increasing the TEOS/PEO_{114}-*b*-PLA_{173} ratio to 5 : 1 led to the formation of scattering peaks in a specific peak ratio of 1 : $\sqrt{3}$: $\sqrt{4}$, suggesting the development of a representative hexagonal cylindrical packing structure, as confirmed through TEM imaging [Fig. 5(j)]. Further increasing the TEOS/PEO_{114}-*b*-PLA_{173} ratio to 10 : 1 resulted in a SAXS pattern featuring a peak ratio of 1 : $\sqrt{7}$, indicating the development of a representative hexagonal cylindrical packing structure, as confirmed by the TEM image in Fig. 5(k). When the TEOS/PEO_{114}-*b*-PLA_{173} ratios were 15 : 1 and 20 : 1, SAXS analyses revealed only single broad peaks, indicating the near-disordered and short/long-ordered morphologies of disordered spherical and micelle structures, respectively, as confirmed through TEM imaging [Fig. 5(k)], similar to those formed using our other two PEO-*b*-PLA diblock copolymer templates.

Fig. 7 presents N_2 sorption isotherms of the mesoporous silicas we prepared at various TEOS-to-PEO-*b*-PLA weight ratios, using our three PEO-*b*-PLA copolymers (PEO_{114}-*b*-PLA_{73}, PEO_{114}-*b*-PLA_{130}, PEO_{114}-*b*-PLA_{173}) as templates. According to

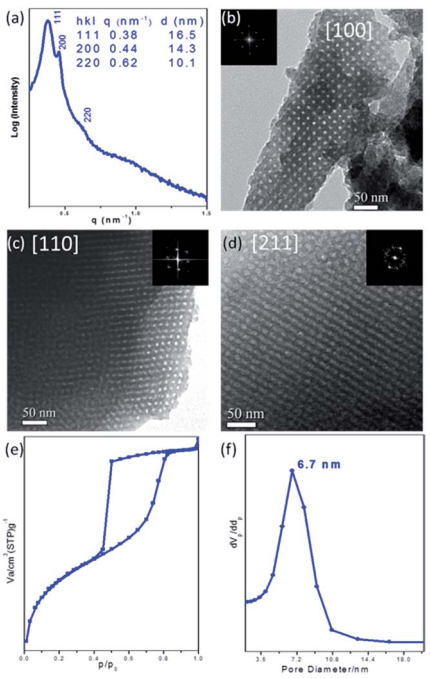

Fig. 6 (a) SAXS, (b–d) TEM, (e) BET adsorption/desorption data, and (f) BET pore size distribution data for the mesoporous silica templated by PEO_{114}-*b*-$PLLA_{130}$ at a TEOS/PEO_{114}-*b*-$PLLA_{130}$ ratio of 10 : 1.

Published on 23 February 2015. Downloaded by National Sun Yat Sen University on 21/04/2015 09:55:25.

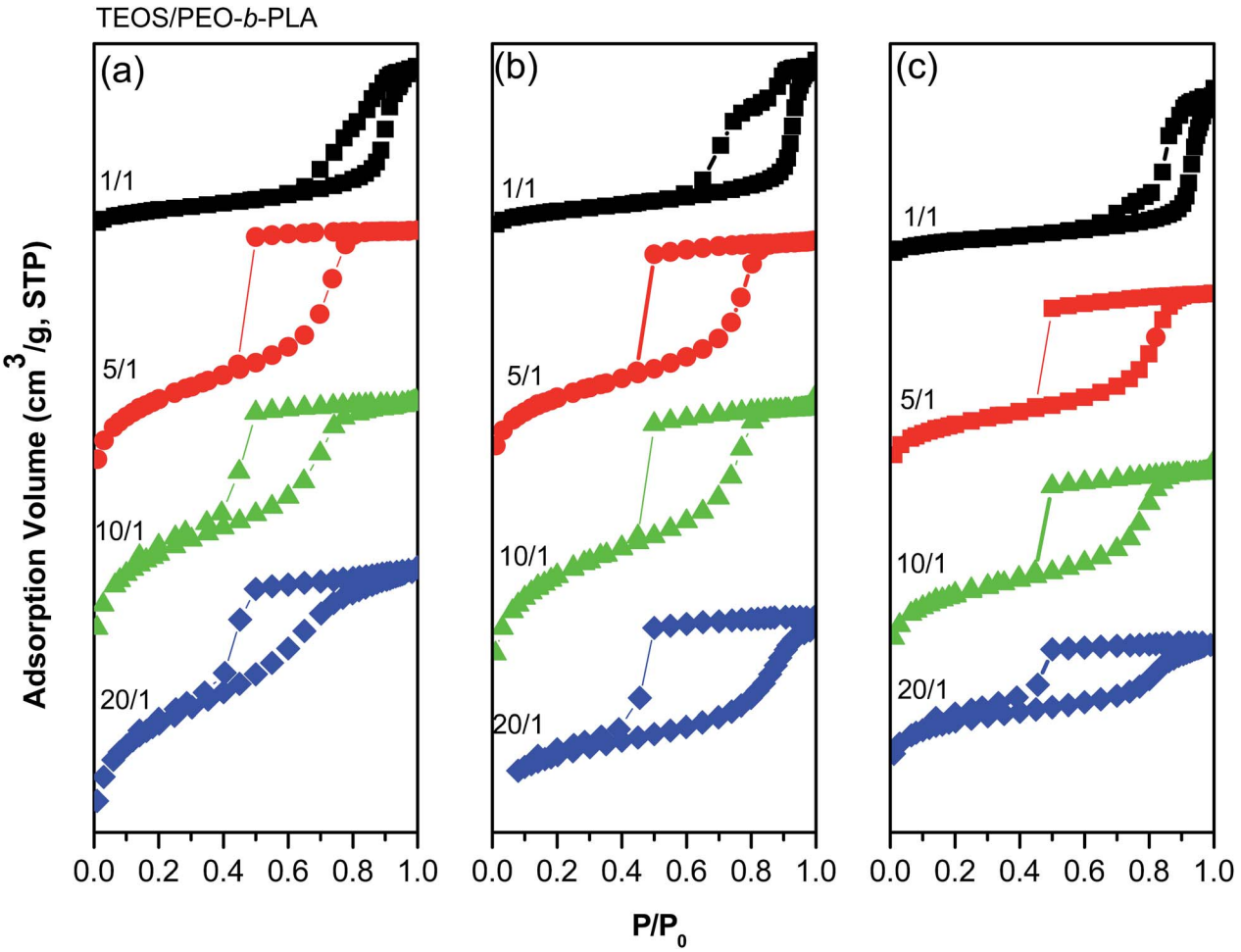

Fig. 7 BET adsorption/desorption data of mesoporous silicas templated by the diblock copolymers (a) PEO_{114}-*b*-PLA_{73}, (b) PEO_{114}-*b*-PLA_{130}, and (c) PEO_{114}-*b*-PLA_{173}.

the Brunauer–Deming–Deming–Teller (BDDT) classification system, the mesoporous silica samples all provided typical type-IV isotherms in their N_2 adsorption/desorption curves.[43] The mesoporous silica samples prepared using the three templates at a TEOS/PEO-*b*-PLA ratio of 1 : 1 all underwent a capillary condensation step in the relative pressure range from 0.6 to 1.0, thereby exhibiting typical H_3-like hysteresis loops, indicating broad pore size distributions centered from 19 to 28 nm (based on the Harkins–Jura model) that increased upon increasing the PLA molecular weight in the PEO-*b*-PLA copolymers (Fig. 8). For TEOS/PEO-*b*-PLA ratios of 5 : 1 and 10 : 1, H_2-like hysteresis loops appeared at values of P/P_0 from 0.4 to 0.8, characteristic of spherical mesopores; here, we calculated the pore size distributions from the adsorption branches, based on the spherical BdB model. Fig. 8 also reveals that the average pore sizes in the mesoporous silica samples prepared using TEOS/PEO-*b*-PLA = 5 : 1 increased from 5.7 to 7.3 to 9.5 nm, while those prepared using TEOS/PEO-*b*-PLA = 10 : 1 increased from 5.2 to 7.1 to 7.8 nm, upon increasing the molecular weight of the PLA block in the PEO-*b*-PLA copolymer. We also found the pore volume and pore size was generally decreased with the increase of TEOS ratios since the TEOS will interact with PEO segment and this

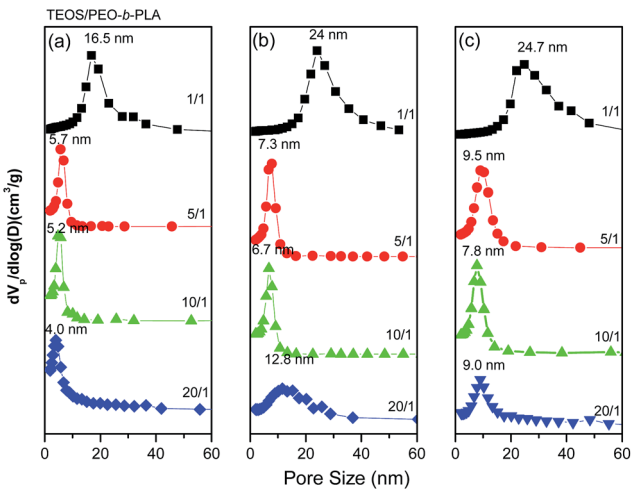

Fig. 8 BET pore size distribution data of mesoporous silicas templated by the diblock copolymers (a) PEO_{114}-*b*-PLA_{73}, (b) PEO_{114}-*b*-PLA_{130}, and (c) PEO_{114}-*b*-PLA_{173}.

This journal is © The Royal Society of Chemistry 2015

Published on 23 February 2015. Downloaded by National Sun Yat Sen University on 21/04/2015 09:55:25.

will increase the thickness of wall and decreases the pore size. As a result, the pore volume will shrink in this case. Similar results are also observed in previous PEO-*b*-PCL block copolymer as templates.[23,27] A further increase the TEOS/PEO-*b*-PLA ratio to 20 : 1 also resulted in an H_2-like hysteresis with a disordered micelle structure, but the variation in average pore size did not follow any obvious trend. As a result, we could obtain well-defined ordered mesoporous silicas when using PEO-*b*-PLA diblock copolymers as templates at TEOS/PEO-*b*-PLA ratios of 1 : 1, 5 : 1, and 10 : 1. These structures are quite different from the lamellar mesoporous structures we obtained when using PEO-*b*-PLLA diblock copolymers as templates.

Comparison of crystalline/crystalline PEO-*b*-PLLA and crystalline/amorphous PEO-*b*-PLA diblock copolymer templates

In crystalline/crystalline block copolymers, there are two factors that determine their final phase and crystalline morphology: microphase separation of the diblock copolymer and crystallization of the crystallizable block(s). When we used PEO-*b*-PLLA diblock copolymers as templates, where crystallization was favored over microphase separation, we obtained only lamellar mesoporous structures. Fig. 9 presents SAXS patterns of mesoporous silicas templated by PEO-*b*-PLLA and PEO-*b*-PLA having the same molecular weights for their PLLA and PLA block segments. The pattern in Fig. 9(a), for the structure templated by TEOS/PEO_{114}-*b*-$PLLA_{130}$ = 1 : 1, features its maximum intensity at a value of q^* of approximately 0.31 nm^{-1} (d = 20.3 nm); a disordered lamellar structure appears in the corresponding TEM image [Fig. 10(a) and (b)]. Further increasing the weight ratio of TEOS/PEO_{114}-*b*-$PLLA_{130}$ to 5 : 1, 10 : 1, and 15 : 1 caused the primary SAXS peak to gradually shift to lower values of q^* and become broader, indicating that the d-spacing gradually grew to 28.5 nm and that the mesoporous silicas became more disordered. These features were also evident in the TEM images in Fig. 10(c)–(h), with the mesoporous structures revealing more typical lamellar character upon increasing the TEOS content. For the mesoporous silica samples templated by the $EO_{114}LLA_{130}$ template, it was evident that the PLLA segment was more likely to crystallize and form lamellar structures, rather than form a microphase separation-induced self-assembled morphology.[37] In contrast, eliminating the crystalline ability of the PLLA block segment by installing an amorphous PLA block segment led to long-range order at a q/q_{max} ratio of 1 : $\sqrt{3}$: $\sqrt{4}$, corresponding to the long-range order of a hexagonally packed cylinder structure, as confirmed using TEM [Fig. 10(i) and (j)]; further increasing the TEOS/PEO-*b*-PLA ratio to 5 : 1 led to a weak peak ratio of 1 : $\sqrt{3}$: $\sqrt{4}$, also corresponding to the hexagonally packed cylinder structure, as revealed through TEM [Fig. 10(k) and (l)]. Notably, further increasing the TEOS/PEO-*b*-PLA ratio to 10 : 1 led to an FCC

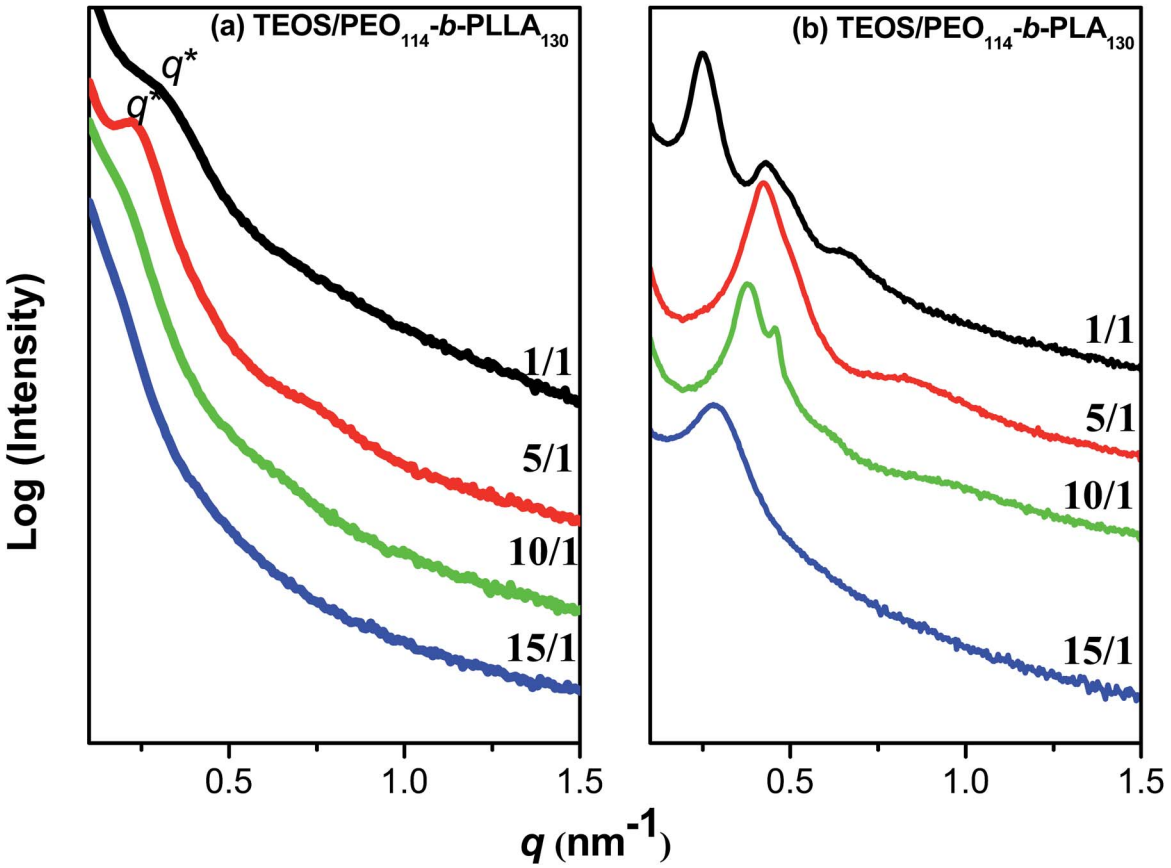

Fig. 9 SAXS patterns of mesoporous silicas templated by (a) PEO_{114}-*b*-$PLLA_{130}$ and (b) PEO_{114}-*b*-PLA_{130}.

Published on 23 February 2015. Downloaded by National Sun Yat Sen University on 21/04/2015 09:55:25.

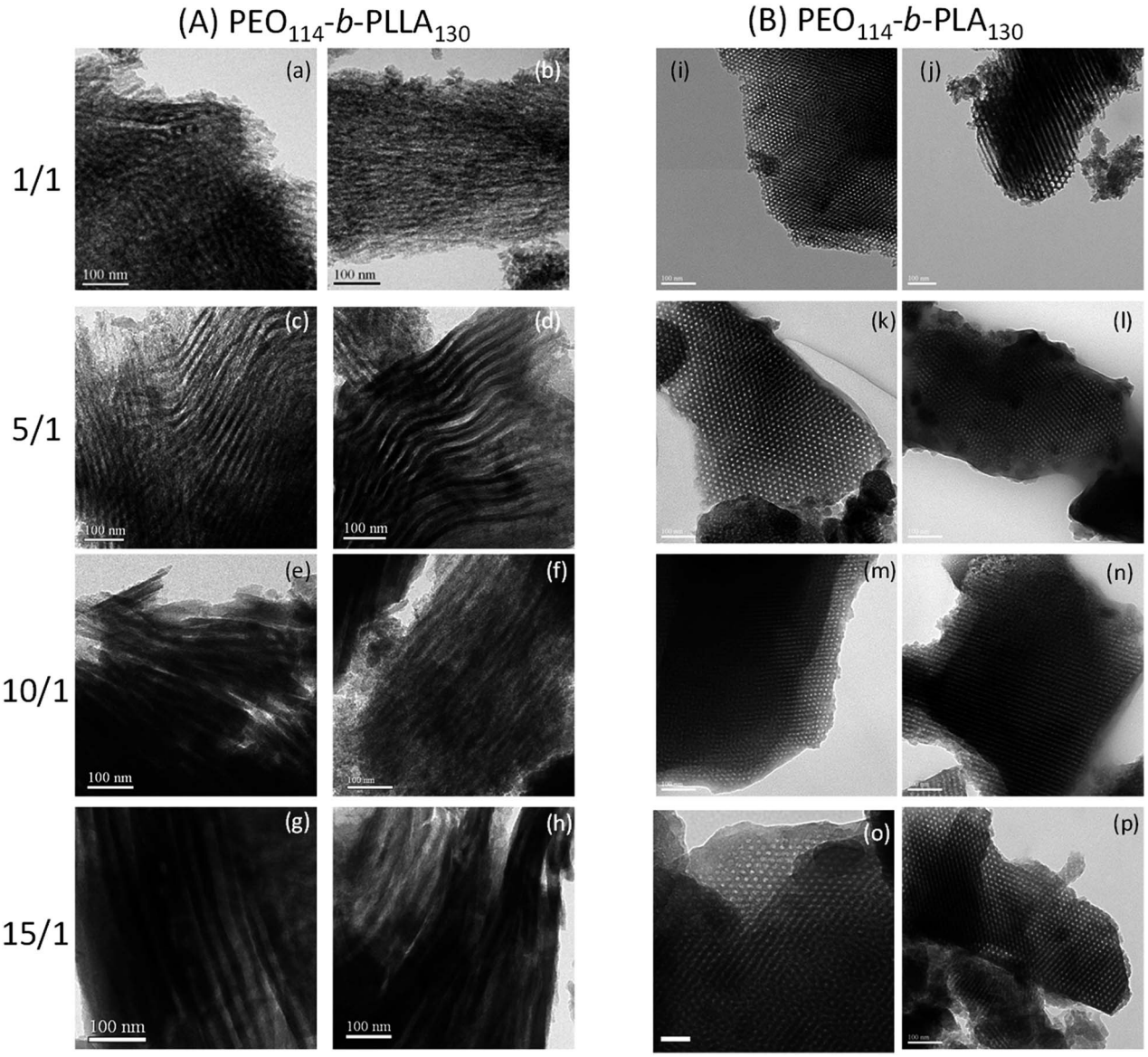

Fig. 10 TEM images of mesoporous silicas templated by (A) PEO_{114}-*b*-$PLLA_{130}$ and (B) PEO_{114}-*b*-PLA_{130}.

lattice, identified through characteristic peak positions at a relative ratio of $1 : \sqrt{4/3} : \sqrt{8/3}$ and confirmed by the TEM image in Fig. 10(m) and (n) as well as Fig. 6(b)–(d). When the TEOS/PEO-*b*-PLA ratio was 15 : 1, only a single broad peak appeared through SAXS analysis, indicating the near-disordered and short/long-ordered morphologies of a disordered spherical and micelle structure, as revealed in Fig. 10(o) and (p).

Fig. 11 presents N_2 sorption isotherms of mesoporous silicas templated by PEO-*b*-PLLA and PEO-*b*-PLA having the same molecular weights of their PLLA and PLA block segments. The mesoporous silica samples prepared at the different TEOS-to-PEO_{114}-*b*-$PLLA_{130}$ weight ratios all provided typical type-IV isotherms in their N_2 adsorption/desorption curves [Fig. 11(a)]. They all exhibited H_3-like hysteresis loops at values of P/P_0 ranging from 0.75 to 0.95, indicative of typical mesoporous structures with slit-like pores (distorted lamellar pores). Fig. 11(c) displays the mean pore sizes measured from the adsorption branches, based on the Harkins–Jura model. The mesopore size increased from 17.7 to 32.1 nm upon increasing the TEOS-to-$EO_{114}LLA_{130}$ weight ratio, but the corresponding pore size distributions became broader. The mesoporous silica samples prepared at the different TEOS-to-PEO_{114}-*b*-PLA_{130} weight ratios also all provided typical type-IV isotherms in their N_2 adsorption/desorption curves [Fig. 11(c)]. At a TEOS/PEO-*b*-PLA ratio of 1 : 1, they all displayed typical H_1-like hysteresis loops, consistent with cylindrical mesoporous structures. For TEOS/PEO-*b*-PLA ratios of 5 : 1, 10 : 1, and 15 : 1, they all revealed H_2-like hysteresis loops at values of P/P_0 from 0.4 to 0.8, characteristic of spherical mesopores; we calculated the pore size distributions from the adsorption branches, based on the spherical BdB model. In contrast to the behavior of the PEO-*b*-PLLA templates, here the mesopore size decreased from

 This journal is © The Royal Society of Chemistry 2015

Published on 23 February 2015. Downloaded by National Sun Yat Sen University on 21/04/2015 09:55:25.

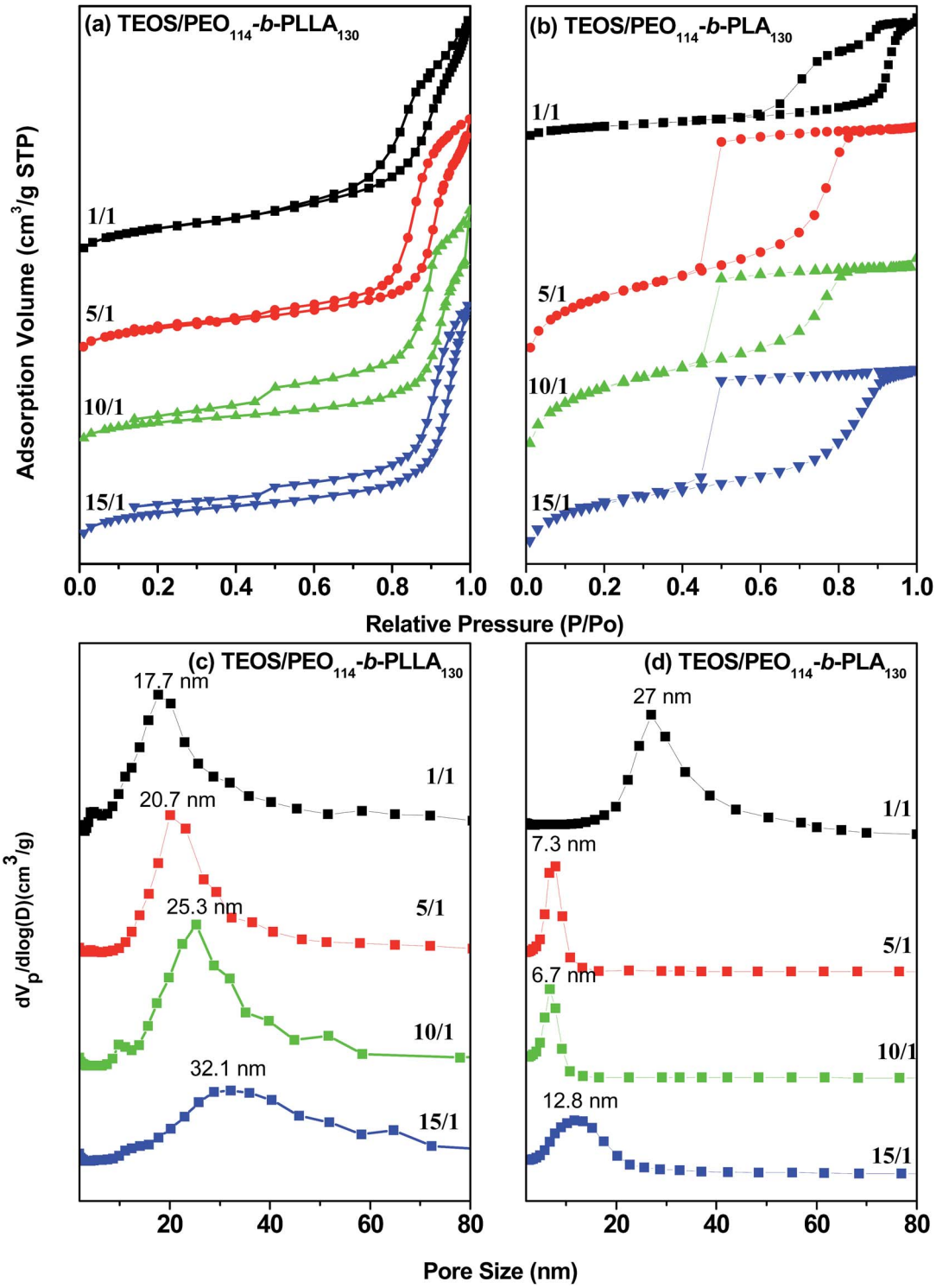

Fig. 11 (a and b) BET adsorption/desorption data and (c and d) pore size distributions of mesoporous silicas templated by (a and c) PEO_{114}-*b*-$PLLA_{130}$ and (b and d) PEO_{114}-*b*-PLA_{130}.

27.7 to 7.1 nm upon increasing the TEOS-to-$EO_{114}LA_{130}$ weight ratio from 1 : 1 to 10 : 1, with the corresponding pore size distributions narrowing, indicating that well-defined ordered structures could be obtained. Further increasing the ratio of TEOS-to-$EO_{114}LA_{130}$ to 15 : 1 led to a slight increase in the mesopore size, to 12.8 nm. In addition, the sizes of the mesopores templated by PEO-*b*-PLA decreased significantly when compared with those obtained using PEO-*b*-PLLA of the same molecular weight at higher TEOS/template ratios. The PEO-*b*-PLA diblock copolymers used as templates also provided

Published on 23 February 2015. Downloaded by National Sun Yat Sen University on 21/04/2015 09:55:25.

more ordered structures. Most importantly, the PEO-*b*-PLA diblock copolymers used as templates exhibited an order–order transition of their mesoporous structures upon changing the ratio of TEOS to EO_{114}-*b*-PLA_{130}.

Conclusions

We have prepared mesoporous silica materials through EISA when employing PEO-*b*-PLA diblock copolymers as templates at various TEOS/PEO-*b*-PLA ratios and at various volume fractions of the PLA block segment. We found that crystallization was the key effect in the preparation of mesoporous silica templated by PLLA. Indeed, when using PEO-*b*-PLLA diblock copolymers as templates, where crystallization of the PLLA block segment was favored over microphase separation, we obtained only lamellar mesoporous structures. In contrast, after removing the crystallization ability of the PLLA block segment, replacing it with an amorphous PLA block segment, we obtained a series of long-range-ordered mesoporous silicas. As a result, we propose another key effect of crystallization ability for preparation of highly ordered mesoporous silicas having large pores and this study could be extended to other system when consider the crystallization effect of these diblock copolymers.

Acknowledgements

This study was supported financially by the Ministry of Science and Technology, Republic of China, under contracts MOST 100-2221-E-110-029-MY3 and MOST 102-2221-E-110-008-MY3. We thank Mr Hsien-Tsan Lin of the Regional Instruments Center, National Sun Yat-Sen University, for help with the TEM experiments.

References

1 H. A. Klok and S. Lecommandoux, *Adv. Mater.*, 2001, **13**, 1217–1229.
2 Y. Mai and A. Eisenberg, *Chem. Soc. Rev.*, 2012, **41**, 5969–5985.
3 G. J. A. A. Soler-Illia and O. Azzaroni, *Chem. Soc. Rev.*, 2011, **40**, 1107–1150.
4 Y. Deng, J. Wei, Z. Sun and D. Zhao, *Chem. Soc. Rev.*, 2013, **42**, 4054–4070.
5 W. Li and D. Zhao, *Chem. Commun.*, 2013, **49**, 943–946.
6 D. Y. Zhao, J. L. Feng, Q. S. Huo, N. Melosh, G. H. Fredrickson, B. F. Chmelka and G. D. Stucky, *Science*, 1998, **279**, 548–552.
7 D. Y. Zhao, Q. S. Huo, J. L. Feng, B. F. Chmelka and G. D. Stucky, *J. Am. Chem. Soc.*, 1998, **120**, 6024–6036.
8 M. Kruk, M. Jaroniec, C. H. Ko and R. Ryoo, *Chem. Mater.*, 2000, **12**, 1961–1968.
9 K. C. W. Wu, X. Jiang and Y. Yamauchi, *J. Mater. Chem.*, 2011, **21**, 8934–8939.
10 G. Soler-Illia, A. Louis and C. Sanchez, *Chem. Mater.*, 2002, **14**, 750–759.
11 D. Grosso, C. Boissiere, B. Smarsly, T. Brezesinski, N. Pinna, P. A. Albouy, H. Amenitsch, M. Antonietti and C. Sanchez, *Nat. Mater.*, 2004, **3**, 787–792.
12 C. J. Brinker, Y. F. Lu, A. Sellinger and H. Y. Fan, *Adv. Mater.*, 1999, **11**, 579–585.
13 Y. F. Lu, H. Y. Fan, A. Stump, T. L. Ward, T. Rieker and C. J. Brinker, *Nature*, 1999, **398**, 223–226.
14 D. Grosso, F. Cagnol, G. Soler-Illia, E. L. Crepaldi, H. Amenitsch, A. Brunet-Bruneau, A. Bourgeois and C. Sanchez, *Adv. Funct. Mater.*, 2004, **14**, 309–322.
15 Y. Deng, T. Yu, Y. Wan, Y. Shi, Y. Meng, D. Gu, L. Zhang, Y. Huang, C. Liu, X. Wu and D. Zhao, *J. Am. Chem. Soc.*, 2007, **129**, 1690–1697.
16 Y. Deng, J. Liu, C. Liu, D. Gu, Z. Sun, J. Wei, J. Zhang, L. Zhang, B. Tu and D. Zhao, *Chem. Mater.*, 2008, **20**, 7281–7286.
17 E. Bloch, P. L. Llwewllyn, T. Phan, D. Bertin and V. Hornebecq, *Chem. Mater.*, 2009, **21**, 48–55.
18 G. Ma, X. Yan, Y. Li, L. Xiao, Z. Huang, Y. Lu and J. Fan, *J. Am. Chem. Soc.*, 2010, **132**, 9596–9597.
19 D. Chandra, T. Ohji, K. Kato and T. Kimura, *Phys. Chem. Chem. Phys.*, 2011, **13**, 12529–12535.
20 D. Chandra, M. Bekki, M. Nakamura, S. Sonezaki, T. Ohji, K. Kato and T. Kimura, *J. Mater. Chem.*, 2011, **21**, 5738–5744.
21 J. Wei, Y. Deng, J. Zhang, Z. Sun, B. Tu and D. Zhao, *Solid State Sci.*, 2011, **13**, 784–792.
22 Y. Deng, C. Liu, D. Gu, T. Yu, B. Tu and D. Zhao, *J. Mater. Chem.*, 2008, **18**, 91–97.
23 B. C. Garcia, M. Kamperman, R. Ulrich, A. Jain, S. M. Gruner and U. Wiesner, *Chem. Mater.*, 2009, **21**, 5397–5405.
24 S. W. Kuo, C. L. Lin and F. C. Chang, *Macromolecules*, 2002, **35**, 278–285.
25 J. G. Li and S. W. Kuo, *RSC Adv.*, 2011, **1**, 1822–1833.
26 J. G. Li, Y. D. Lin and S. W. Kuo, *Macromolecules*, 2011, **44**, 9295–9309.
27 J. G. Li, R. B. Lin and S. W. Kuo, *Macromol. Rapid Commun.*, 2012, **33**, 678–682.
28 J. G. Li, C. Y. Chuang and S. W. Kuo, *J. Mater. Chem.*, 2012, **22**, 18583–18595.
29 J. G. Li, Y. H. Chang, Y. S. Lin and S. W. Kuo, *RSC Adv.*, 2012, **2**, 12973–12982.
30 W. C. Chu, J. G. Li and S. W. Kuo, *RSC Adv.*, 2013, **3**, 6485–6498.
31 J. G. Li, R. B. Lin and S. W. Kuo, *RSC Adv.*, 2013, **3**, 17411–17423.
32 J. G. Li, W. C. Chu, U. S. Jeng and S. W. Kuo, *Macromol. Chem. Phys.*, 2013, **214**, 2115–2123.
33 W. C. Chu, S. F. Chiang, J. G. Li and S. W. Kuo, *RSC Adv.*, 2014, **4**, 784–793.
34 C. C. Liu, J. G. Li and S. W. Kuo, *RSC Adv.*, 2014, **4**, 20262–20272.
35 C. C. Liu, J. G. Li, W. C. Chu and S. W. Kuo, *Macromolecules*, 2014, **47**, 6389–6400.
36 W. C. Chu, C. X. Lin and S. W. Kuo, *RSC Adv.*, 2014, **4**, 61012–61021.
37 J. G. Li, W. C. Chu, C. W. Tu and S. W. Kuo, *J. Nanosci. Nanotechnol.*, 2013, **13**, 2495–2506.

 This journal is © The Royal Society of Chemistry 2015

38 J. H. Chang, K. J. Kim and Y. K. Shin, *Bull. Korean Chem. Soc.*, 2004, **25**, 351–356.
39 J. H. Chang, C. H. Shim, K. J. Kim and B. S. Bae, *J. Ind. Eng. Chem.*, 2005, **11**, 471–474.
40 B. Nandan, J. Y. Hsu and H. L. Chen, *J. Macromol. Sci. Polymer Rev.*, 2006, **46**, 143–172.
41 K. Rezwan, Q. Z. Chen, J. J. Blaker and A. R. Boccaccini, *Biomaterials*, 2006, **27**, 3413–3431.
42 R. V. Castillo, A. J. Muller, J. M. Raquez and P. Dubois, *Macromolecules*, 2010, **43**, 4149–4160.
43 Q. Li, B. Guo, J. Yu, J. Ran, B. Zhang, H. Yan and J. R. Gong, *J. Am. Chem. Soc.*, 2011, **133**, 10878–10884.

Published on 23 February 2015. Downloaded by National Sun Yat Sen University on 21/04/2015 09:55:25.